Fusion of Evidences in Intensities Channels for Edge Detection in PolSAR Images

Journal:	*Geoscience and Remote Sensing Letters*
Manuscript ID	GRSL-00400-2020.R1
Manuscript Type:	Recent Advances in Geoscience and Remote Sensing: Technologies, Standards, and Applications
Sub-topic:	Image Processing, Analysis and Classification
Date Submitted by the Author:	n/a
Complete List of Authors:	DE BORBA, ANDERSON; Ibmec São Paulo, Economy; Mackenzie Presbyterian University, Dept. Engenharia Elétrica e Computação, Marengoni, Maurício; Mackenzie Presbyterian University, Dept. Engenharia Elétrica e Computação Frery, Alejandro; Universidade Federal de Alagoas, Laboratório de Computação Científica e Análise Numérica (LaCCAN)
Key Words:	SAR Data < Processing, Sensors and Systems for, Electromagnetics and Remote Sensing, Radar Data < Processing, Sensors and Systems for

Fusion of Evidences in Intensities Channels for Edge Detection in PolSAR Images

Revision R1

Anderson A de Borba, Maurício Marengoni, and Alejandro C. Frery, *Senior Member, IEEE*

I. Editor-in-Chief

Comment #1

Your manuscript GRSL-00400-2020 Fusion of Evidences in Intensities Channels for Edge Detection in PolSAR Images has been reviewed by the GRSL Editorial Review Board and found to be not acceptable without major revisions.

It is recommended that you revise your paper and resubmit it in accordance with the Editorial Review Board comments given below. Complete instructions for submitting a revision can be found at the bottom of this letter.

Thank you very much for handling this manuscript.

We have prepared a revised version taking into account all the comments and suggestions made by the reviewers.

In fact, we found the reviews well-informed and constructive, and we would like to thank the reviewers, the Associate Editor, and Prof. Avik Bhattacharya for helping us make a better contribution.

This response letter addresses all the comments in red, followed by our reactions, and, whenever necessary, the changes made.

We also include the `diff` article between the prior and current versions, where deletions are in red and additions are in blue.

As a final comment, we would like to stress that we added a link to a repository with the code and data that promote the reproducibility of this work; cf. Sec. V-D.

II. Associate Editor

Comment #1

Both reviewers have given valuable comments and suggested that a major revision is necessary.

Thank you very much. To the best of our knowledge, we have addressed all the comments and suggestions.

III. Reviewer #1

Comment #1

This paper discusses the fusion of evidences in PolSAR images for the edge detection. Here are some suggestions.

In the abstract, “fusion of evidence” should be “fusion of evidences”. “in the intensity (hh), (hv), and (vv) channels” should be “in the intensity channels (hh, hv and vv)”.

Thank you very much for this suggestion. We made the changes, as requested:

Changes #1

The present study discusses an edge detection method based on the fusion of ~~evidence~~ evidences obtained in the intensity channels hh, hv, and vv in the intensity ~~(hh), (hv), and (vv) channels~~of PolSAR multi-look images.

Comment #2

In the introduction part, the paragraph “We adopted the Gambini Algorithm...”,what is the purpose to use Gambini Algorithm? It should be elaborated to help the reader understand.

We added a rationale for the choice of this Algorithm:

Changes #2

~~We adopted the~~ The Gambini Algorithm [1] ~~, which~~ is an attractive edge detection technique. It is local, as it finds evidence of an edge over a thin strip of data; it works with any model, which makes it suitable for SAR data; and it has shown better performance than other approaches. This algorithm consists in casting rays, and then finding the evidence of an edge in the ray by maximizing a value function.

Comment #3

More detailed description for Gambini Algorithm in Section III is suggested.

Thank you very much for this suggestion. We made the changes and put the algorithm 1, as requested:

Changes #3

~~We approach edge detection with the Gambini Algorithm [2]–[4]. It consists of the following steps:~~

1) ~~Identify the centroid of a region of interest (ROI) in an automatic, semi-automatic or manual manner.~~
2) ~~Cast rays from the centroid to the outside of the area.~~
3) ~~Collect data on a strip, ideally of the size of a pixel, around the rays using the Bresenham's midpoint line algorithm.~~
4) ~~Compute the value functionon every point of the ray.~~
5) ~~Use the GenSA method [5], to find points of maxima in the functions of interest.~~
6) ~~Fuse the evidence of detected edges in the (hh), (hv) and (vv) channels.~~

The Gambini algorithm estimates the point at which the properties of a sample change. It has been used with stochastic distances [4], and with the likelihood function [2], [3] for edge detection in SAR/PolSAR imagery. It can be adapted to any suitable measure of dissimilarity between two samples.

The ~~value function is the reduced log-likelihood of the inner and external samples of the strip denoted, respectively, as z_{I} and z_{E}. Each strip~~ algorithm starts by casting rays from a point inside the candidate region, e.g., the centroid. Data are collected around each ray to form the sample $\boldsymbol{z} = (z_1, z_2, \ldots, z_n)$~~is, thus, partitioned in two disjoint samples~~, which is partitioned at position j:

~~The~~ We then compute the total log-likelihood ~~at point j is, then,~~ of $\boldsymbol{z}_{\mathrm{I}}$ and $\boldsymbol{z}_{\mathrm{E}}$:

$$\begin{aligned}\mathcal{L}(j;\widehat{\mu}_I,\widehat{L}_I,\widehat{\mu}_E,\widehat{L}_E) = -\left(\frac{\widehat{L}_{\mathrm{I}}}{\widehat{\mu}_{\mathrm{I}}}\sum_{k=1}^{j} z_k + \frac{\widehat{L}_{\mathrm{E}}}{\widehat{\mu}_{\mathrm{E}}}\sum_{k=j+1}^{n} z_k\right) + \\ j\left[\widehat{L}_{\mathrm{I}}\ln(\widehat{L}_{\mathrm{I}}/\widehat{\mu}_{\mathrm{I}}) - \ln\Gamma(\widehat{L}_{\mathrm{I}})\right] + \widehat{L}_{\mathrm{I}}\sum_{k=1}^{j}\ln z_k + \\ (n-j)\left[\widehat{L}_{\mathrm{E}}\ln(\widehat{L}_{\mathrm{E}}/\widehat{\mu}_{\mathrm{E}}) - \ln\Gamma(\widehat{L}_{\mathrm{E}})\right] + \widehat{L}_{\mathrm{E}}\sum_{k=j+1}^{n}\ln z_k.\end{aligned} \tag{1}$$

Changes #3- continue

~~We then apply GenSA to find~~

$$\widehat{j} = \arg \max_{j \in [\min_s, N - \min_s]} \ell(j; \widehat{\mu}_I, \widehat{L}_I, \widehat{\mu}_E, \widehat{L}_E),$$

~~where $\min_s$ is a~~ and the estimate of the edge position on the ray is the coordinate $\widehat{j}$ which maximizes it.

Algorithm 1 is the pseudocode of the basic edge detection with the Gambini Algorithm. We found that one hundred rays is a good compromise between spatial continuity and computational load. Also, $\min_s$ is the minimum sample size~~that we set to 14.~~.

~~In this way, we obtain one estimates for the edge for each intensity channel. Notice that this approach can be extended and/or modified to cope with any kind of data.~~

~~We will see ways of fusing these evidences in the next section~~

In our implementation, we replace the exhaustive sequential search (the innermost **for** loop) by Generalized Simulated Annealing (GenSA [5]).

Comment #4

For Eq. (1), the meaning of variable L should be explained. On Page 2, what is the meaning of "we will estimate L on each sample" ?

Thank you very much for noticing this omission. We now clarify the meaning of L and of its local estimation:

Changes #4

Multi-looked fully polarimetric data follow the Wishart distribution with PDF defined by:

$$f_{\mathbf{Z}}(\mathbf{Z}; \mathbf{\Sigma}, L) = \frac{L^{mL}|\mathbf{Z}|^{L-m}}{|\mathbf{\Sigma}|^{L}\Gamma_m(L)} \frac{L^{pL}|\mathbf{z}|^{L-p}}{|\mathbf{\Sigma}|^{L}\Gamma_p(L)} \exp(-L\,\mathrm{tr}(\mathbf{\Sigma}^{-1}\mathbf{Z})), \tag{2}$$

where ~~,~~ $\mathbf{z}$ is a positive-definite Hermitian matrix, L is the number of looks, $\mathrm{tr}(\cdot)$ is the trace operator of a matrix, ~~$\Gamma_m(L)$~~ $\Gamma_p(L)$ is the multivariate Gamma function defined by ~~$\Gamma_m(L) = \pi^{\frac{1}{2}m(m-1)} \prod_{i=0}^{m-1} \Gamma(L-i)$~~ $\Gamma_p(L) = \pi^{\frac{1}{2}p(p-1)} \prod_{i=0}^{p-1} \Gamma(L-i)$, and $\Gamma(\cdot)$ is the Gamma function. We used three ~~$m = 3$~~ $p = 3$ channels in this study. This situation is denoted by $\mathbf{Z} \sim W(\mathbf{\Sigma}, L)$, which satisfies $E[\mathbf{Z}] = \mathbf{\Sigma}$. This assumption usually holds ~~on targets where the speckle is fully developed~~ for fully developed speckle but, since we will estimate L ~~on each sample (~~locally instead of considering the same number of looks for the whole image~~)~~, we will in part take into account departures from such hypothesis.

Comment #5

On Page 2, what is the meaning of "we will estimate L on each sample" ?

Thank you very much for this suggestion. We better explain how we estimate the L in each sample.

Changes #5

This assumption usually holds ~~on targets where the speckle is fully developed~~ for fully developed speckle but, since we will estimate L ~~on each sample (~~locally instead of considering the same number of looks for the whole image~~)~~, we will in part take into account departures from such hypothesis.

Comment #6

In Section IV, different symbol for $\ell = mn$ should be used to distinguish the ℓ in Eq. (3).

Thank you very much for your careful reading. In fact, we used the same symbol for two different entities. We opted for denoting the likelihood with $\mathcal{L}$, and keeping ℓ for the image size. The equations that changed appear highlighted in the `diff` manuscript.

Comment #7

What is the relationship between and m, n, c and n_c? Make it clear.

We now explain the notation more clearly:

Changes #7

~~Denote in the following $\widehat{\boldsymbol{j}}_c$ the binary image with same support as the input data c (m lines and n columns; denote $\ell = mn$), where~~ Assume we have n_c binary images $\{\widehat{\boldsymbol{j}}_c\}_{1\leq c\leq n_c}$ in which 1 denotes an estimate of edge and 0 otherwise. ~~We have n_c of these image to fuse, and the result of the fusion will be denoted~~ They have common size $m \times n$; denote $\ell = mn$. These images will be fused to obtain the binary image $\boldsymbol{I}_F$.

Comment #8

In Section III-A, the meaning of (x, y) should be explained.

We now explain that these are the image coordinates:

Changes #8

The simple average fusion method proposes the arithmetic mean of the edge evidence in each of the n_c channels: $\boldsymbol{I}_F(x, y) = (n_c)^{-1} \sum_{c=1}^{n_c} \widehat{\boldsymbol{j}}_c(x, y)$, where $1 \leq x \leq m$ indexes the rows, and $1 \leq y \leq n$ the columns of the image.

Comment #9

In Section V-A Line 16, correct the "Fig. 1a" and "Fig. 1b".

Thank you very much. Corrected.

Comment #10

What is the meaning of "$\ell(4)$" in Section V-A?

This was unclear, indeed; thanks for noticing. The new version states:

Changes #10

It is worth noting that GenSA has accurately identified the maximum value of ~~ℓ~~$\mathcal{L}$ (Eq. (8)), even in the presence of multiple local maxima.

Comment #11

For the experiments, more examples are suggested to verify the conclusion.

Changes #11

We have inserted two more cases, the first considering another region of interest in Flevoland's image. Figures 4(a) and (b) show the region of interest and figure (5) the detection of edge evidence for each channel. The twp best edge evidences fusions are shown in figure (6). For the second region using the San Francisco bay image, we show the region of interest in figure (7) and the edge detection for each channel in figure (8). The two best edge evidences fusions are shown in figure (8).

Comment #12

"Synthetic Polarimetric Aperture Radar (PolSAR)" should be "Polarimetric Synthetic Aperture Radar (PolSAR)"

Corrected. Thank you very much.

IV. Reviewer #2

Comments to the Author The paper present an edge detection method based on the fusion of evidence obtained on the difference channels of Polarimetric SAR images. The paper is well written and organized. It is easy to follow. The theoretical aspects are well presented. The bibliography is adequate for Letter. The main concern I have is related to experimental results. Even if interesting and well presented, the considered test cases are limited.

Comment #1

In my opinion, the authors should consider the possibility of showing other test cases. Generally speaking, one single test case is not enough to draw conclusions. Therefore, I encourage the authors to consider at least one other test-case (preferably other two). The authors could reduce the size of the presented images, in order to have enough space. A deeper discussion of the obtained results should be considered.

The authors thank the reviewer for the suggestions, which contributed to improve the quality of the article.

Changes #1

We have inserted two more cases, the first considering another region of interest in Flevoland's image. Figures 4(a) and (b) show the region of interest and figure (5) the detection of edge evidence for each channel. The twp best edge evidences fusions are shown in figure (6). For the second region using the San Francisco bay image, we show the region of interest in figure (7) and the edge detection for each channel in figure (8). The two best edge evidences fusions are shown in figure (8).

V. ANOTHERS CHANGES

Changes #1 - Abstract

The fusion methods used are: simple average, multi-resolution discrete wavelet transform (MR-DWT)~~and stationary (MR-SWT) wavelet transforms~~, principal component analysis (PCA), ROC statistics, multi-resolution stationary (MR-SWT) wavelet transform, and a multi-resolution method based on singular value decomposition (MR-SVD). A quantitative analysis suggests that ~~MR-SWT provides~~ PCA and MR-SVD provide the best results.

Changes #2 - Introduction

Among the available edge detection techniques for SAR and PolSAR images, it is worth mentioning: techniques based on denoising ~~[6]–[10];~~ [6]–[8], [10]; Markov random fields [11]; the deep learning approach ~~[12], [13]~~ [13] applied to segmentation and classification; and ~~,~~ statistical techniques [2]–[4] applied in edge detection in PolSAR ~~/~~ and SAR imagery.

This article follows the statistical modeling approach using the techniques described in [2]–[4] to find edge evidences, followed by fusion processes [14], [15]. ~~Our approach does not attempt to reduce the speckle, but to extract information from its statistical properties.~~

Changes #3 - Introduction

~~The value function we use is the~~ We use the total likelihood of two samples: one inside the edge, another outside the edge. Without loss of generality, we assume the complex scaled Wishart distribution for the fully polarimetric observations ~~[16]~~, from which Gamma laws stem for each intensity channel. The value function depends on the estimates that index such Gamma laws~~. We~~ ; and we estimate them by maximum likelihood~~with the BFGS optimization method implemented in the `maxLik` package [17]~~.

The ~~value function is the total likelihood . It~~ total likelihood function is non-differentiable at most points~~in the domain. It is known that~~ , and classical methods have difficulties in finding ~~the maximumof a non-differentiable functions~~its maximum. We used the Generalized Simulated Annealing (GenSA) [5] method to solve this problem.

Changes #4 - Introduction

We discuss and compare six fusion methods: Simple average [14], Multi-Resolution Discrete Wavelet, MR-DWT [18], Principal Component Analysis, PCA [14], [18], ROC statistics ~~[19], [20] ,~~ [19], Multi-Resolution Stationary Wavelet Transform, MR-SWT [18], [21], and Multi-Resolution Singular Value Decomposition, MR-SVD [22].

Changes #5 - Introduction

The article is structured as follows. Section VIII describes ~~statistical modeling~~the models. Section IX describes ~~edge detection for PolSAR data~~the edge detection. Section X describes the ~~approach to edge evidence fusing~~ approaches for fusing edge evidences. Section XI presents ~~numerical results. Finally,~~ the results. In Section XII ~~concludes the work with observations, future directions of research , and the feasibility of detecting edges in each channel of PolSAR images~~we discuss the results, and outline future research directions.

Changes #6 - Section II

~~Fully polarimetric data may be modeled by .~~ Since we are interested in describing the information conveyed by parts of such matrix ~~, we rely on the results presented in [23], [24]. In particular~~under the Wishart model, we assume that the distribution of each intensity channel is a Gamma law with probability density function

$$f_Z(z;\mu,L) = \frac{L^L z^{L-1}}{\mu^L \Gamma(L)} \exp\{-Lz/\mu\}, \quad z>0, \tag{3}$$

where $L>0$~~(rather than $L \geq 1$ to allow for flexibility)~~, and $\mu>0$ is the mean.

~~Given~~ The log-likelihood of the sample $\boldsymbol{z}=(z_1,\ldots,z_n)$ ~~, the reduced log-likelihood of~~ under this model is

$$\ell\mathcal{L}(\boldsymbol{z};L,\mu) = n[L\ln(L/\mu) - \ln\Gamma(L)] + L\sum_{k=1}^{n}\ln z_k - \frac{L}{\mu}\sum_{k=1}^{n} z_k. \tag{4}$$

We obtain ~~$(\widehat{L},\widehat{\mu})$~~$(\widehat{L},\widehat{\mu})$, the maximum likelihood estimator (MLE) of (L,μ) based on $\boldsymbol{z}$, by maximizing (7) with the BFGS method~~implemented in the `maxLik` package~~ [17]. We prefer optimization to solving $\nabla\ell=\mathbf{0}$ for improved numerical stability.

Changes #7 - Section IV

We, thus, use two resolution levels.

Changes #8 - Section IV

The result of the fusion I_F is the inverse DWT ~~transformation~~ transform of the coefficient matrices $\bar{\boldsymbol{J}}_{c\mathrm{HH}}$, $\bar{\boldsymbol{J}}_{c\mathrm{LL}}$, $\bar{\boldsymbol{J}}_{c\mathrm{LH}}$, and $\bar{\boldsymbol{J}}_{c\mathrm{HL}}$.

Changes #9 - Section IV

1) Compute the ~~components $\boldsymbol{P}_c = (\sum_{m=1}^{n_c}\boldsymbol{V}_c(m))^{-1}\boldsymbol{V}_c$, where $\boldsymbol{V}_c$~~ vector $\boldsymbol{P}=(P(1),\ldots,P(n_c)) = (\sum_{c=1}^{n_c}V(c))^{-1}\boldsymbol{V}$, where $\boldsymbol{V}$ is eigenvector associated with the highest eigenvalue of ~~$\boldsymbol{X}\boldsymbol{C}_{n_c\times n_c}$~~; notice that ~~$\sum_{c=1}^{n_c}\boldsymbol{P}_c = 1$~~$\sum_{c=1}^{n_c}P(c)=1$.
2) Fuse ~~$\boldsymbol{I}_F(x,y) = \sum_{c=1}^{n_c}\boldsymbol{P}_c\widehat{\boldsymbol{J}}_c(x,y)$~~$\boldsymbol{I}_F(x,y) = \sum_{c=1}^{n_c}P(c)\widehat{\boldsymbol{J}}_c(x,y)$.

Changes #10 - Section IV

The ROC method was proposed and described on ~~[19], [20]~~ [19]:

Changes #11 - Section IV

This section is based on [18], [21]. The difference between MR-DWT and MR-SWT method is the replacement of the ~~method discrete wavelet transform~~ Discrete Wavelet Transform (DWT) by the ~~method stationary wavelet transform~~ Stationary Wavelet Transform SWT.

Changes #12 - Section IV

MR-SVD Fusion [22] works similarly to MR-DWT. ~~The difference consists in changing the DWT filters by the SVD filters. The~~ The MR-SVD fusion method can be summarized as follows:

Changes #13 - Section IV

1) Find the SVD decomposition of $\boldsymbol{X}_1 = \boldsymbol{U}_1 \boldsymbol{S}_1 \boldsymbol{V}_1^T$, where $\boldsymbol{U}_1$ ~~and $\boldsymbol{V}_1$ are unitary and they have dimensions~~ is a 4×4 ~~e $\ell/4 \times \ell/4$ respectively. The diagonal entries S_{ii} of~~ unitary matrix, $\boldsymbol{S}_1$ ~~are known as the singular values of $\boldsymbol{X}_1$ and it have dimension~~ is a $4 \times \ell/4$ rectangular diagonal matrix known as singular values matrix, and $\boldsymbol{V}_1$ is an $\ell/4 \times \ell/4$ unitary matrix. The singular values are ~~sorted in descending, and they are putting in the diagonal principal of the matrix, other entries must be zeros~~ordered in a decreasing order.

We also used two resolution levels.

Changes #14 - Section V

A. ~~PolSAR image~~Flevoland images

~~We used~~ Fig. 1(a) shows a 750×1024 pixels AIRSAR PolSAR image of Flevoland, L-band, ~~for the tests. Fig. 1a shows the ROI,~~ with the radial lines where edges are detected. Fig. ~~1b~~ 1(b) shows the ground reference in red.

Changes #15 - Section V

~~The simple~~ Simple average and PCA produce similar results. MR-SVD produces considerably less outliers than the other methods~~, at the cost of longer processing time~~.

Changes #16 - Section V

Fig. 4 shows another region in the Flevoland image. In this case, it is a bright target surrounded by darker fields. Fig. 5 shows the edges detected in each intensity channel and, again, the hv data are the one which produce the most accurate results.

Changes #17 - Section V

Fig. 6 shows the two best fusion results: PCA and MR-SVD. Notice that the latter (Fig. 6(b)) eliminates the wrong detection close to the center of the area, and has fewer wrongly detected points outside the region of interest.

Changes #18 - Section V

B. San Francisco Image

Fig. 7 shows an area of an L-band AIRSAR image over San Francisco. The distinctive areas are urban, sea, and vegetation. The aim is finding the edge between the former and the other two.

Changes #19 - Section V

Fig. 8 shows the evidences of edges found in each of the three intensity channels. A visual inspection suggests that the hh channel is the one that produces the best estimation.

Changes #20 - Section V

Fig. 9 shows the two best fusion results: PCA and MR-SVD. Again, the latter is more resistant to outliers, both inside and outside the region of interest.

Changes #21 - Section V

C. Error analysis

Figure 10 shows the error of $\widehat{j}$ in finding the true edge shown in Fig. 1(b), as measured on 100 ~~radial lines :~~ lines with the minimum Euclidean distance ~~among~~ between the ground truth ~~pixel and the several pixels detected~~ and the detected pixel in the fusion methods. We use relative frequencies to estimate the probability of having an error smaller than a number of pixels. Denoting $H(k)$ the number of ~~replications~~ lines for which the error is less than k pixels, an estimate of this probability is $f(k) = H(k)/n_r$, where n_r is ~~the radial number~~ number of lines. In our analysis, k varies between 1 and 10, and $n_r = 100$. The algorithm is described in Ref. [3].

Changes #22 - Section V

D. Implementation Details

~~The system presented here was executed on a Intel© Core i7-9750HQ CPU 2.6 GHz 16 GB RAM computer. The method for detecting edge evidence MLE was implemented in the R language. The fusion methods were implemented in Matlab.~~

Table I shows the running times (absolute and relative to the fastest method). The system presented here was executed on a Intel© Core i7-9750HQ CPU 2.6 GHz 16 GB RAM computer.

Changes #23 - Section V

The method for detecting edge evidence MLE was implemented in the R language. The fusion methods were implemented in Matlab. Code and data are available at https://github.com/anderborba/Code_GRSL_2020_1.

Changes #24 - Section VI

We found evidence of edges using the maximum likelihood method under the Wishart model for PolSAR data. The evidence was found in each of the three intensity channels of ~~an~~ AIRSAR L-band ~~image over Flevoland~~ images over Flevoland and San Francisco.

Changes #25 - Section VI

~~The~~ Over the agricultural fields of Flevoland, the best edge evidence was observed on the hv channel. ~~We assessed the result by checking the closeness of the fused points to the actual edge, by the presence of outliers, and by the blurring effect~~The hh channel provided the best estimates of the edges between the urban and both sea and vegetation areas of San Francisco. Such diversity of information content justifies the need of fusing the edge evidences.

Changes #26 - Section VI

The best ~~result was produced by~~ results were produced by PCA and by the Multi-Resolution ~~Stationary Wavelet Transform (MR-SWT)with a moderate cost of the~~ Singular Value Decomposition (MR-SVD). Such enhancement comes at additional computational cost in terms of processing time.

Changes #27 - Section VI

We ~~highlight two~~ quantitatively assessed the results by checking the closeness of the fused points to the actual edge, and by the presence of outliers. Although the average and PCA are similar with respect to the probability of correctly detecting the edge, the latter provides a more effective weight of the evidences. In fact, PCA is able to completely discard misleading evidences, while the average cannot.

Changes #28 - Section VI

Two avenues for future improvement of the fusion ~~:~~ are: (1) increasing the number of evidences. This is possible, since fully polarimetric data ~~is~~ are richer than mere intensity channels; and (2) post-processing of both partial evidences and fusion.

VI. Difference between the article submitted and the last version sent to GRSL

Abstract

~~Synthetic Polarimetric~~ Polarimetric Synthetic Aperture Radar (PolSAR) sensors have reached an essential position in remote sensing. The images they provide have speckle noise, making their processing and analysis challenging tasks. ~~The present study discusses~~ We discuss an edge detection method based on the fusion of ~~evidence~~ evidences obtained in the intensity ~~(hh), (hv), and (vv) channels~~ channels hh, hv, and vv of PolSAR multi-look images. The method consists of detecting transition points in the thinnest possible range of data that covers two regions using maximum likelihood under the Wishart distribution. The fusion methods used are: simple average, multi-resolution discrete wavelet transform (MR-DWT)~~and stationary (MR-SWT) wavelet transforms~~, principal component analysis (PCA), ROC statistics, multi-resolution stationary (MR-SWT) wavelet transform, and a multi-resolution method based on singular value decomposition (MR-SVD). A quantitative analysis suggests that ~~MR-SWT provides~~ PCA and MR-SVD provide the best results.

Index Terms

PolSAR, edge detection, maximum likelihood estimation, fusion methods.

VII. Introduction

Polarimetric synthetic aperture radar (PolSAR) has achieved an essential position ~~as a remote sensingtechnology~~in remote sensing. The data such sensors provide require specifically tailored signal processing techniques. Among such techniques, edge detection is one of the most important operations for extracting information.

Edges are at a higher level of abstraction than mere data and, as such, provide relevant insights about the scene.

Among the available edge detection techniques for SAR and PolSAR images, it is worth mentioning: techniques based on denoising ~~[6]–[10];~~ [6]–[8], [10]; Markov random fields [11]; the deep learning approach ~~[12], [13]~~ [13] applied to segmentation and classification; and ~~,~~ statistical techniques [2]–[4] applied in edge detection in PolSAR ~~/~~ and SAR imagery.

This article follows the statistical modeling approach using the techniques described in [2]–[4] to find edge evidences, followed by fusion processes [14], [15]. ~~Our approach does not attempt to reduce the speckle, but to extract information from its statistical properties.~~

Instead of handling fully polarimetric data, we treat each intensity channel separately, obtain evidence of edges, and then produce a single estimator of the edge position. With this, we quantify the contribution each channel provides to the solution of the problem.

~~We adopted the~~ The Gambini Algorithm [1] ~~, which~~ is an attractive edge detection technique. It is local, as it finds evidence of an edge over a thin strip of data; it works with any model, which makes it suitable for SAR data; and it has shown better performance than other approaches. This algorithm consists in casting rays, and then finding the evidence of an edge in the ray by maximizing a value function. ~~The value function we use is the~~ We use the total likelihood of two samples: one inside the edge, another outside the edge. Without loss of generality, we assume the complex scaled Wishart distribution for the fully polarimetric observations ~~[16]~~, from which Gamma laws stem for each intensity channel. The value function depends on the estimates that index such Gamma laws. ~~We~~ ; and we estimate them by maximum likelihood~~with the BFGS optimization method implemented in the `maxLik` package [17]~~.

The ~~value function is the total likelihood . It~~ total likelihood function is non-differentiable at most points~~in the domain. It is known that~~ , and classical methods have difficulties in finding ~~the maximumof a non-differentiable functions~~its maximum. We used the Generalized Simulated Annealing (GenSA) [5] method to solve this problem.

We discuss and compare six fusion methods: Simple average [14], Multi-Resolution Discrete Wavelet, MR-DWT [18], Principal Component Analysis, PCA [14], [18], ROC statistics ~~[19], [20],~~ [19], Multi-Resolution Stationary Wavelet Transform, MR-SWT [18], [21], and Multi-Resolution Singular Value Decomposition, MR-SVD [22].

The article is structured as follows. Section VIII describes ~~statistical modeling~~the models. Section IX describes ~~edge detection for PolSAR data~~the edge detection. Section X describes the ~~approach to edge evidence fusing~~ approaches for fusing edge evidences. Section XI presents ~~numerical results. Finally,~~ the results. In Section XII ~~concludes the work with observations, future directions of research , and the~~

feasibility of detecting edges in each channel of PolSAR imageswe discuss the results, and outline future research directions.

VIII. Statistical modeling for PolSAR data

Multi-looked fully polarimetric data follow the Wishart distribution with PDF defined by:

$$f_{\mathbf{Z}}(\mathbf{Z}\underline{\mathbf{z}};\boldsymbol{\Sigma},L)=\frac{L^{mL}|\mathbf{Z}|^{L-m}}{|\boldsymbol{\Sigma}|^{L}\Gamma_m(L)}\frac{L^{pL}|\mathbf{z}|^{L-p}}{|\boldsymbol{\Sigma}|^{L}\Gamma_p(L)}\exp(-L\,\mathrm{tr}(\boldsymbol{\Sigma}^{-1}\mathbf{Z}\underline{\mathbf{z}})), \tag{5}$$

where , $\mathbf{z}$ is a positive-definite Hermitian matrix, L is the number of looks, $\mathrm{tr}(\cdot)$ is the trace operator of a matrix, $\Gamma_m(L)$ $\Gamma_p(L)$ is the multivariate Gamma function defined by $\Gamma_m(L)=\pi^{\frac{1}{2}m(m-1)}\prod_{i=0}^{m-1}\Gamma(L-i)$ $\Gamma_p(L)=\pi^{\frac{1}{2}p(p-1}$ and $\Gamma(\cdot)$ is the Gamma function. We used three $m=3$ $p=3$ channels in this study. This situation is denoted by $\mathbf{Z}\sim W(\boldsymbol{\Sigma},L)$, which satisfies $E[\mathbf{Z}]=\boldsymbol{\Sigma}$. This assumption usually holds on targets where the speckle is fully developed for fully developed speckle but, since we will estimate L on each sample (locally instead of considering the same number of looks for the whole image), we will in part take into account departures from such hypothesis.

Fully polarimetric data may be modeled by . Since we are interested in describing the information conveyed by parts of such matrix , we rely on the results presented in [23], [24]. In particularunder the Wishart model, we assume that the distribution of each intensity channel is a Gamma law with probability density function

$$f_Z(z;\mu,L)=\frac{L^L z^{L-1}}{\mu^L\Gamma(L)}\exp\{-Lz/\mu\},\quad z>0, \tag{6}$$

where $L>0$(rather than $L\geq 1$ to allow for flexibility), and $\mu>0$ is the mean.

Given The log-likelihood of the sample $\boldsymbol{z}=(z_1,\ldots,z_n)$, the reduced log-likelihood of under this model is

$$\ell\mathcal{L}(\underline{z}\underline{\boldsymbol{z}};L,\mu)=n\big[L\ln(L/\mu)-\ln\Gamma(L)\big]+L\sum_{k=1}^{n}\ln z_k-\frac{L}{\mu}\sum_{k=1}^{n}z_k. \tag{7}$$

We obtain $(\widehat{L},\widehat{\mu})$ $(\widehat{L},\widehat{\mu})$, the maximum likelihood estimator (MLE) of (L,μ) based on $\boldsymbol{z}$, by maximizing (7) with the BFGS methodimplemented in the `maxLik` package [17]. We prefer optimization to solving $\nabla\ell=\mathbf{0}$ for improved numerical stability.

IX. Edge Detection on a Single Data Strip

We approach edge detection with the Gambini Algorithm [2]–[4]. It consists of the following steps:

1) Identify the centroid of a region of interest (ROI) in an automatic, semi-automatic or manual manner.
2) Cast rays from the centroid to the outside of the area.

3) ~~Collect data on a strip, ideally of the size of a pixel, around the rays using the Bresenham's midpoint line algorithm.~~
4) ~~Compute the value functionon every point of the ray.~~
5) ~~Use the GenSA method [5], to find points of maxima in the functions of interest.~~
6) ~~Fuse the evidence of detected edges in the (hh), (hv) and (vv) channels.~~

The Gambini algorithm estimates the point at which the properties of a sample change. It has been used with stochastic distances [4], and with the likelihood function [2], [3] for edge detection in SAR/PolSAR imagery. It can be adapted to any suitable measure of dissimilarity between two samples.

The ~~value function is the reduced log-likelihood of the inner and external samples of the strip denoted, respectively, as z_{I} and z_{E}. Each strip~~ algorithm starts by casting rays from a point inside the candidate region, e.g., the centroid. Data are collected around each ray to form the sample $\boldsymbol{z} = (z_1, z_2, \ldots, z_n)$~~is, thus, partitioned in two disjoint samples~~, which is partitioned at position j:

$$\boldsymbol{z} = (\underbrace{z_1, z_2, \ldots, z_j}_{\boldsymbol{z}_{\mathrm{I}}}, \underbrace{z_{j+1}, z_{j+2}, \ldots, z_n}_{\boldsymbol{z}_{\mathrm{E}}}).$$

We assume two (possibly) different models for each partition: $\boldsymbol{Z}_{\mathrm{I}} \sim \Gamma(\mu_{\mathrm{I}}, L_{\mathrm{I}})$, and $\boldsymbol{Z}_{\mathrm{E}} \sim \Gamma(\mu_{\mathrm{E}}, L_{\mathrm{E}})$. We then estimate $(\mu_{\mathrm{I}}, L_{\mathrm{I}})$ and $(\mu_{\mathrm{E}}, L_{\mathrm{E}})$ with $\boldsymbol{z}_{\mathrm{I}}$ and $\boldsymbol{z}_{\mathrm{E}}$, respectively, by maximizing (7), and obtain ~~$(\widehat{\mu}_{\mathrm{I}}, \widehat{L}_{\mathrm{I}})$ and $(\widehat{\mu}_{\mathrm{E}}, \widehat{L}_{\mathrm{E}})$~~ $(\widehat{\mu}_{\mathrm{I}}, \widehat{L}_{\mathrm{I}})$ and $(\widehat{\mu}_{\mathrm{E}}, \widehat{L}_{\mathrm{E}})$.

~~The~~ We then compute the total log-likelihood ~~at point j is, then,~~ of $\boldsymbol{z}_{\mathrm{I}}$ and $\boldsymbol{z}_{\mathrm{E}}$:

$$\begin{aligned}\mathcal{L}(j; \widehat{\mu}_I, \widehat{L}_I, \widehat{\mu}_E, \widehat{L}_E) = -\left(\frac{\widehat{L}_{\mathrm{I}}}{\widehat{\mu}_{\mathrm{I}}} \sum_{k=1}^{j} z_k + \frac{\widehat{L}_{\mathrm{E}}}{\widehat{\mu}_{\mathrm{E}}} \sum_{k=j+1}^{n} z_k\right) + \\ j\left[\widehat{L}_{\mathrm{I}} \ln(\widehat{L}_{\mathrm{I}}/\widehat{\mu}_{\mathrm{I}}) - \ln\Gamma(\widehat{L}_{\mathrm{I}})\right] + \widehat{L}_{\mathrm{I}} \sum_{k=1}^{j} \ln z_k + \\ (n-j)\left[\widehat{L}_{\mathrm{E}} \ln(\widehat{L}_{\mathrm{E}}/\widehat{\mu}_{\mathrm{E}}) - \ln\Gamma(\widehat{L}_{\mathrm{E}})\right] + \widehat{L}_{\mathrm{E}} \sum_{k=j+1}^{n} \ln z_k.\end{aligned} \tag{8}$$

~~We then apply GenSA to find~~

$$\widehat{j} = \arg \max_{j \in [\min_s, N - \min_s]} \ell(j; \widehat{\mu}_I, \widehat{L}_I, \widehat{\mu}_E, \widehat{L}_E),$$

~~where $\min_s$ is a~~ and the estimate of the edge position on the ray is the coordinate $\widehat{j}$ which maximizes it.

Algorithm 1 is the pseudocode of the basic edge detection with the Gambini Algorithm. We found that one hundred rays is a good compromise between spatial continuity and computational load. Also, $\min_s$ is the minimum sample size~~that we set to 14.~~.

~~In this way, we obtain one estimates for the edge for each intensity channel. Notice that this approach can be extended and/or modified to cope with any kind of data.~~

~~We will see ways of fusing these evidences in the next section~~

Data: n_c intensity channels, interior point, number of rays
Result: n_c binary images with evidences of edges
for *each band* $1 \leq c \leq n_c$ **do**
  for *each ray passing through the interior point* **do**
    $\boldsymbol{z} = (z_1, z_2, \ldots, z_n) \leftarrow$ data collected around the ray;
    for *each* $\min_s \leq j \leq n - \min_s$ **do**
      Partition the sample as $\boldsymbol{z}_{\mathrm{I}} = (z_{\min_s}, \ldots, z_j)$ and $\boldsymbol{z}_{\mathrm{E}} = (z_{j+1}, \ldots, z_{n-\min_s})$;
      Compute $(\widehat{\mu}_{\mathrm{I}}, \widehat{L}_{\mathrm{I}})$ with $\boldsymbol{z}_{\mathrm{I}}$, and $(\widehat{\mu}_{\mathrm{E}}, \widehat{L}_{\mathrm{E}})$ with $\boldsymbol{z}_{\mathrm{E}}$;
      Compute the total log-likelihood at j as $\mathcal{L}(j; \widehat{\mu}_I, \widehat{L}_I, \widehat{\mu}_E, \widehat{L}_E)$;
    end
    $\widehat{\jmath} \leftarrow$ the value of j which maximizes the total log-likelihood function;
    return $(\widehat{x}, \widehat{y})$, the coordinates of each $\widehat{\jmath}$;
  end
  return the binary image $\widehat{\boldsymbol{\jmath}}_c$ with 1 at every $(\widehat{x}, \widehat{y})$, and 0 otherwise.
end

Algorithm 1: Gambini algorithm for intensity channels

In our implementation, we replace the exhaustive sequential search (the innermost **for** loop) by Generalized Simulated Annealing (GenSA [5]).

X. Fusion of Evidences

~~Denote in the following $\widehat{\boldsymbol{\jmath}}_c$ the binary image with same support as the input data c (m lines and n columns; denote $\ell = mn$), where~~ Assume we have n_c binary images $\{\widehat{\boldsymbol{\jmath}}_c\}_{1 \leq c \leq n_c}$ in which 1 denotes an estimate of edge and 0 otherwise. ~~We have n_c of these image to fuse, and the result of the fusion will be denoted~~ They have common size $m \times n$; denote $\ell = mn$. These images will be fused to obtain the binary image $\boldsymbol{I}_F$.

We compare the results of six fusion techniques~~, namely~~: simple average, multi-resolution discrete wavelet transform (MR-DWT), principal components analysis (PCA), ROC statistics, multi-resolution stationary wavelet transform (MR-SWT), and multi-resolution singular value decomposition (MR-SVD).

A. Simple Average

The simple average fusion method proposes the arithmetic mean of the edge evidence in each of the n_c channels: $\boldsymbol{I}_F(x,y) = (n_c)^{-1}\sum_{c=1}^{n_c}\widehat{\boldsymbol{\jmath}}_c(x,y)$, where $1 \le x \le m$ indexes the rows, and $1 \le y \le n$ the columns of the image.

B. Multi-Resolution Discrete Wavelet – MR-DWT

This section is based on [18]. We apply DWT filters on each binary image $\widehat{\boldsymbol{\jmath}}_c$: a low-pass filter $\boldsymbol{L}$ in the vertical direction, and a high-pass filter $\boldsymbol{H}$ in the horizontal direction, then both are down-sampled to create the coefficient matrices $\widehat{\boldsymbol{\jmath}}_{c\mathrm{L}}$ and $\widehat{\boldsymbol{\jmath}}_{c\mathrm{H}}$. These operations are repeated on the coefficient matrices, leading to $\widehat{\boldsymbol{\jmath}}_{c\mathrm{LL}}$, $\widehat{\boldsymbol{\jmath}}_{c\mathrm{LH}}$, $\widehat{\boldsymbol{\jmath}}_{c\mathrm{HL}}$, and $\widehat{\boldsymbol{\jmath}}_{c\mathrm{HH}}$. We, thus, use two resolution levels.

The DWT fusion method has the following steps:

1) Calculate the DWT decomposition $\widehat{\boldsymbol{\jmath}}_{c\mathrm{LL}}$, $\widehat{\boldsymbol{\jmath}}_{c\mathrm{LH}}$, $\widehat{\boldsymbol{\jmath}}_{c\mathrm{HL}}$, and $\widehat{\boldsymbol{\jmath}}_{c\mathrm{HH}}$, for each channel.
2) Compute $\bar{\boldsymbol{\jmath}}_{c\mathrm{HH}}$, the pixel-wise mean of all $\widehat{\boldsymbol{\jmath}}_{c\mathrm{HH}}$ decompositions.
3) Find the pixel-wise maximum of $\widehat{\boldsymbol{\jmath}}_{c\mathrm{LL}}$, $\widehat{\boldsymbol{\jmath}}_{c\mathrm{LH}}$, $\widehat{\boldsymbol{\jmath}}_{c\mathrm{HL}}$: $\bar{\boldsymbol{\jmath}}_{c\mathrm{LL}}$, $\bar{\boldsymbol{\jmath}}_{c\mathrm{LH}}$, and $\bar{\boldsymbol{\jmath}}_{c\mathrm{HL}}$.
4) The result of the fusion I_F is the inverse DWT ~~transformation~~ transform of the coefficient matrices $\bar{\boldsymbol{\jmath}}_{c\mathrm{HH}}$, $\bar{\boldsymbol{\jmath}}_{c\mathrm{LL}}$, $\bar{\boldsymbol{\jmath}}_{c\mathrm{LH}}$, and $\bar{\boldsymbol{\jmath}}_{c\mathrm{HL}}$.

C. Principal Component Analysis – PCA

This section is based on [14], [18]. The method is comprised of the following steps:

1) Stack the binary images $\widehat{\boldsymbol{\jmath}}_c$ in column vectors to obtain the matrix $\boldsymbol{X}_{\ell\times n_c}$.
2) Calculate the covariance matrix $\boldsymbol{C}_{n_c\times n_c}$ of $\boldsymbol{X}_{\ell\times n_c}$.
3) Compute the matrices of eigenvalues ($\boldsymbol{\Lambda}$) and eigenvectors ($\boldsymbol{V}$) of the covariance matrix, sorted in decreasing order by the eigenvalues.
4) Compute the ~~components $\boldsymbol{P}_c = (\sum_{m=1}^{n_c}\boldsymbol{V}_c(m))^{-1}\boldsymbol{V}_c$, where $\boldsymbol{V}_c$~~ vector $\boldsymbol{P} = (P(1),\ldots,P(n_c)) = (\sum_{c=1}^{n_c}V(c))^{-1}\boldsymbol{V}$, where $\boldsymbol{V}$ is eigenvector associated with the highest eigenvalue of ~~$\boldsymbol{X}\boldsymbol{C}_{n_c\times n_c}$~~; notice that ~~$\sum_{c=1}^{n_c}\boldsymbol{P}_c = 1$~~ $\sum_{c=1}^{n_c}P(c) = 1$
5) Fuse ~~$\boldsymbol{I}_F(x,y) = \sum_{c=1}^{n_c}\boldsymbol{P}_c\widehat{\boldsymbol{\jmath}}_c(x,y)$~~ $\boldsymbol{I}_F(x,y) = \sum_{c=1}^{n_c}P(c)\widehat{\boldsymbol{\jmath}}_c(x,y)$.

D. ROC Statistics

The ROC method was proposed and described on ~~[19], [20]~~ [19]:

1) Add the binary images $\widehat{\boldsymbol{\jmath}}_c$ to produce the frequency matrix ($\boldsymbol{V}$).
2) Use thresholds ranging from $t = 1,\ldots,n_c$ on $\boldsymbol{V}$ to generate matrices $\boldsymbol{M}_t$.

3) Compare each $\boldsymbol{M}_t$ with all $\widehat{\boldsymbol{j}}_c$, find the confusion matrix to generate the ROC curve. The optimal threshold corresponds to the point of the ROC curve closest (in the sense of the Euclidean distance) to the diagnostic line.
4) The fusion $\boldsymbol{I}_F$ is the matrix $\boldsymbol{M}_t$ which corresponds to the optimal threshold.

E. Multi-Resolution Stationary Wavelet Transform – MR-SWT

This section is based on [18], [21]. The difference between MR-DWT and MR-SWT method is the replacement of the ~~method discrete wavelet transform~~ Discrete Wavelet Transform (DWT) by the ~~method stationary wavelet transform~~ Stationary Wavelet Transform SWT.

F. Multi-Resolution Singular Value Decomposition – MR-SVD

MR-SVD Fusion [22] works similarly to MR-DWT. ~~The difference consists in changing the DWT filters by the SVD filters. The~~ The MR-SVD fusion method can be summarized as follows:

1) Organize the binary image $\widehat{\boldsymbol{j}}_c$ as non-overlapping 2×2 blocks, and arrange each block as a 4×1 vector by stacking columns to form the data matrix $\boldsymbol{X}_1$ with dimension $4 \times \ell/4$.
2) Find the SVD decomposition of $\boldsymbol{X}_1 = \boldsymbol{U}_1 \boldsymbol{S}_1 \boldsymbol{V}_1^T$, where $\boldsymbol{U}_1$ ~~and $\boldsymbol{V}_1$ are unitary and they have dimensions~~ is a 4×4 ~~e $\ell/4 \times \ell/4$ respectively. The diagonal entries S_{ii} of~~ unitary matrix, $\boldsymbol{S}_1$ ~~are known as the singular values of $\boldsymbol{X}_1$ and it have dimension~~ is a $4 \times \ell/4$ rectangular diagonal matrix known as singular values matrix, and $\boldsymbol{V}_1$ is an $\ell/4 \times \ell/4$ unitary matrix. The singular values are ~~sorted in descending, and they are putting in the diagonal principal of the matrix, other entries must be zeros~~ordered in a decreasing order.
3) Transform the lines of $\widehat{\boldsymbol{X}}_1 = \boldsymbol{U}_1^T \boldsymbol{X}_1 = \boldsymbol{S}_1 \boldsymbol{V}_1^T$ into new matrices with dimensions $m/2 \times n/2$: $\{\boldsymbol{\Phi}_1, \boldsymbol{\Psi}_{1\mathrm{V}}, \boldsymbol{\Psi}_{1\mathrm{H}}, \boldsymbol{\Psi}_{1\mathrm{D}}\}$.
4) Repeat the procedure (1) on $\boldsymbol{\Phi}_r$ by $r = 2$ up to the lowest resolution level R.
5) The MR-SVD decomposition in each channel is

$$\widehat{\boldsymbol{X}}_c \rightarrow \left\{ \boldsymbol{\Phi}_{\mathrm{R}}^c, \{\boldsymbol{\Psi}_{r\mathrm{V}}^c, \boldsymbol{\Psi}_{r\mathrm{H}}^c, \boldsymbol{\Psi}_{r\mathrm{D}}^c\}_{r=1}^{\mathrm{R}}, \{\boldsymbol{U}_r^c\}_{r=1}^{\mathrm{R}} \right\}.$$

6) Once the decomposition is applied to all channels, compute the average of $\boldsymbol{\Phi}_R^c$ ($\boldsymbol{\Phi}_{\mathrm{R}}^f$) in the lowest resolution level, and the average of $\boldsymbol{U}_r^c$ ($\boldsymbol{U}_{\mathrm{r}}^f$), for each r, where f denotes the fusion among channels.
7) Find the pixel-wise maxima of $\boldsymbol{\Psi}_{r\mathrm{V}}^c$, $\boldsymbol{\Psi}_{r\mathrm{H}}^c$ and $\boldsymbol{\Psi}_{r\mathrm{D}}^c$: $\boldsymbol{\Psi}_{rV}^f$ $\boldsymbol{\Psi}_{r\mathrm{V}}^f$, $\boldsymbol{\Psi}_{r\mathrm{H}}^f$ and $\boldsymbol{\Psi}_{r\mathrm{D}}^f$.
8) The fusion $\boldsymbol{I}_F$ is the SVD transformation for each level $r = \mathrm{R}, \ldots, 1$,

$$\boldsymbol{I}_F \leftarrow \left\{ \boldsymbol{\Phi}_{\mathrm{R}}^f, \{\boldsymbol{\Psi}_{r\mathrm{V}}^f, \boldsymbol{\Psi}_{r\mathrm{H}}^f, \boldsymbol{\Psi}_{r\mathrm{D}}^f\}_{r=\mathrm{R}}^{1}, \{\boldsymbol{U}_r^f\}_{r=\mathrm{R}}^{1} \right\}.$$

We also used two resolution levels.

XI. Results

A. ~~PolSAR image~~Flevoland images

~~We used~~ Fig. 1(a) shows a 750 × 1024 pixels AIRSAR PolSAR image of Flevoland, L-band, ~~for the tests. Fig. 1a shows the ROI,~~ with the radial lines where edges are detected. Fig. ~~1b~~ 1(b) shows the ground reference in red.

Figs. 2(a), 2(b), and 2(c) show, respectively, the edge evidences in the hh, hv and vv channels as obtained by MLE.

It is worth noting that GenSA has accurately identified the maximum value of ~~ℓ~~$\mathcal{L}$ (Eq. (8)), even in the presence of multiple local maxima. A visual assessment leads to conclude that the best results are provided by hv, although with a few points far from the actual edge.

Figs. 3(a), 3(b), 3(c), 3(d), 3(e), and 3(f) show the results of fusing these evidences.

~~The simple~~ Simple average and PCA produce similar results. MR-SVD produces considerably less outliers than the other methods~~, at the cost of longer processing time~~. ROC produces accurate edges, with few outliers, but sparsely. Both wavelet-based methods (DWT and SWT) produce too dense edges and many outliers.

Fig. 4 shows another region in the Flevoland image. In this case, it is a bright target surrounded by darker fields. Fig. 5 shows the edges detected in each intensity channel and, again, the hv data are the one which produce the most accurate results.

Fig. 6 shows the two best fusion results: PCA and MR-SVD. Notice that the latter (Fig. 6(b)) eliminates the wrong detection close to the center of the area, and has fewer wrongly detected points outside the region of interest.

B. San Francisco Image

Fig. 7 shows an area of an L-band AIRSAR image over San Francisco. The distinctive areas are urban, sea, and vegetation. The aim is finding the edge between the former and the other two.

Fig. 8 shows the evidences of edges found in each of the three intensity channels. A visual inspection suggests that the hh channel is the one that produces the best estimation.

Fig. 9 shows the two best fusion results: PCA and MR-SVD. Again, the latter is more resistant to outliers, both inside and outside the region of interest.

C. Error analysis

Figure 10 shows the error of $\widehat{j}$ in finding the true edge shown in Fig. 1(b), as measured on 100 ~~radial lines :~~ lines with the minimum Euclidean distance ~~among~~ between the ground truth ~~pixel and the several pixels detected~~ and the detected pixel in the fusion methods. We use relative frequencies to estimate the probability of having an error smaller than a number of pixels. Denoting $H(k)$ the number of ~~replications~~ lines for which the error is less than k pixels, an estimate of this probability is $f(k) = H(k)/n_r$, where n_r is ~~the radial number~~ number of lines. In our analysis, k varies between 1 and 10, and $n_r = 100$. The algorithm is described in Ref. [3].

D. Implementation Details

~~The system presented here was executed on a Intel© Core i7-9750HQ CPU 2.6 GHz 16 GB RAM computer. The method for detecting edge evidence MLE was implemented in the R language. The fusion methods were implemented in Matlab.~~

Table I shows the running times (absolute and relative to the fastest method). The system presented here was executed on a Intel© Core i7-9750HQ CPU 2.6 GHz 16 GB RAM computer.

The method for detecting edge evidence MLE was implemented in the R language. The fusion methods were implemented in Matlab. Code and data are available at https://github.com/anderborba/Code_GRSL_2020_1.

XII. Conclusion

We found evidence of edges using the maximum likelihood method under the Wishart model for PolSAR data. The evidence was found in each of the three intensity channels of ~~an~~ AIRSAR L-band ~~image over Flevoland~~ images over Flevoland and San Francisco.

~~The~~ Over the agricultural fields of Flevoland, the best edge evidence was observed on the hv channel. ~~We assessed the result by checking the closeness of the fused points to the actual edge, by the presence of outliers, and by the blurring effect~~The hh channel provided the best estimates of the edges between the urban and both sea and vegetation areas of San Francisco. Such diversity of information content justifies the need of fusing the edge evidences.

We applied simple average, MR-DWT, PCA, ROC, MR-SWT, and MR-SVD fusion methods to aggregate the evidence obtained in the three channels. The best ~~result was produced by~~ results were produced by PCA and by the Multi-Resolution ~~Stationary Wavelet Transform (MR-SWT)with a moderate cost of the~~ Singular Value Decomposition (MR-SVD). Such enhancement comes at additional computational cost in terms of processing time. We ~~highlight two~~ quantitatively assessed the results by checking the

closeness of the fused points to the actual edge, and by the presence of outliers. Although the average and PCA are similar with respect to the probability of correctly detecting the edge, the latter provides a more effective weight of the evidences. In fact, PCA is able to completely discard misleading evidences, while the average cannot.

Two avenues for future improvement of the fusion ~~:~~ are: (1) increasing the number of evidences. This is possible, since fully polarimetric data ~~is~~ are richer than mere intensity channels; and (2) post-processing of both partial evidences and fusion.

REFERENCES

[1] J. Gambini, M. Mejail, J. Jacobo-Berlles, and A. C. Frery, "Accuracy of edge detection methods with local information in speckled imagery," *Statistics and Computing*, vol. 18, no. 1, pp. 15–26, 2008.

[2] J. Gambini, M. Mejail, J. Jacobo-Berlles, and A. C. Frery, "Feature extraction in speckled imagery using dynamic B-spline deformable contours under the G0 model," *Int. J. Remote Sens.*, vol. 27, no. 22, pp. 5037–5059, 2006.

[3] A. C. Frery, J. Jacobo-Berlles, J. Gambini, and M. Mejail, "Polarimetric SAR image segmentation with B-Splines and a new statistical model," *Multidimension. Syst. Signal Process.*, vol. 21, pp. 319–342, 2010.

[4] A. Nascimento, M. Horta, A. Frery, and R. Cintra, "Comparing edge detection methods based on stochastic entropies and distances for PolSAR imagery," *IEEE J. Sel. Topics Appl. Earth Observ. Remote Sens.*, vol. 7, no. 2, pp. 648–663, 2014.

[5] Y. Xiang, S. Gubian, B. Suomela, and J. Hoeng, "Generalized Simulated Annealing for Global Optimization: The GenSA Package," *The R Journal*, vol. 5, no. 1, pp. 13–28, 2013.

[6] J. Shi, H. Jin, and Z. Xiao, "A novel hybrid edge detection method for polarimetric SAR images," *IEEE Access*, vol. 8, pp. 8974–8991, 2020.

[7] B. Liu, Z. Zhang, X. Liu, and W. Yu, "Edge extraction for polarimetric SAR images using degenerate filter with weighted maximum likelihood estimation," *IEEE Geosci. Remote Sens. Lett.*, vol. 11, no. 12, pp. 2140–2144, Dec 2014.

[8] W. Wang, D. Xiang, Y. Ban, J. Zhang, and J. Wan, "Enhanced edge detection for polarimetric SAR images using a directional span-driven adaptive window," *Int. J. Remote Sens.*, vol. 39, no. 19, pp. 6340–6357, 2018.

[9] J. Lee, T. L. Ainsworth, and Y. Wang, "A review of polarimetric SAR speckle filtering," in *2017 IEEE International Geoscience and Remote Sensing Symposium (IGARSS)*, July 2017, pp. 5303–5306.

[10] D. Santana-Cedrés, L. Gomez, L. Alvarez, and A. C. Frery, "Despeckling PolSAR images with a structure tensor filter," *IEEE Geosci. Remote Sens. Lett.*, vol. 17, no. 2, pp. 357–361, Feb 2020.

[11] F. Baselice and G. Ferraioli, "Statistical edge detection in urban areas exploiting SAR complex data," *IEEE Geosci. Remote Sens. Lett.*, vol. 9, no. 2, pp. 185–189, March 2012.

[12] J. E. Ball, D. T. Anderson, and C. S. Chan, "Comprehensive survey of deep learning in remote sensing: theories, tools, and challenges for the community," *J. Appl. Remote Sens.*, vol. 11, no. 04, p. 1, sep 2017.

[13] X. X. Zhu, D. Tuia, L. Mou, G. Xia, L. Zhang, F. Xu, and F. Fraundorfer, "Deep learning in remote sensing: A comprehensive review and list of resources," *IEEE Geosci. Remote Sens. Mag.*, vol. 5, no. 4, pp. 8–36, Dec 2017.

[14] H. Mitchell, *Image Fusion: Theories, Techniques and Applications*. Springer Berlin Heidelberg, 2010.

[15] A. A. de Borba, M. Marengoni, and A. C. Frery, "Fusion of evidences for edge detection in PolSAR images," in *2019 IEEE Recent Advances in Geoscience and Remote Sensing: Technologies, Standards and Applications (TENGARSS)*, Oct 2019, pp. 80–85.

[16] S. N. Anfinsen, A. P. Doulgeris, and T. Eltoft, "Estimation of the equivalent number of looks in polarimetric synthetic aperture radar imagery," *IEEE Trans. Geosci. Remote Sens.*, vol. 47, no. 11, pp. 3795–3809, 2009.

[17] A. Henningsen and O. Toomet, "maxlik: A package for maximum likelihood estimation in R," *Computational Statistics*, vol. 26, no. 3, pp. 443–458, 2011.

[18] V. Naidu and J. Raol, "Pixel-level image fusion using wavelets and principal component analysis," *Defence Science Journal*, vol. 58, pp. 338–352, Mar. 2008.

[19] S. Giannarou and T. Stathaki, "Optimal edge detection using multiple operators for image understanding," *EURASIP Journal on Advances in Signal Processing*, vol. 2011, no. 1, p. 28, Jul 2011.

[20] T. Fawcett, "An introduction to ROC analysis," *Pattern Recogn. Lett.*, vol. 27, no. 8, pp. 861–874, Jun. 2006.

[21] Q. Jiang, X. Jin, S. Lee, and S. Yao, "A novel multi-focus image fusion method based on stationary wavelet transform and local features of fuzzy sets," *IEEE Access*, vol. 5, pp. 20 286–20 302, 2017.

[22] V. Naidu, "Image fusion technique using multi-resolution singular value decomposition," *Defence Science Journal*, vol. 61, no. 5, pp. 479–484, Sep. 2011.

[23] J. S. Lee, K. W. Hoppel, S. A. Mango, and A. R. Miller, "Intensity and phase statistics of multilook polarimetric and interferometric SAR imagery," *IEEE Trans. Geosci. Remote Sens.*, vol. 32, no. 5, pp. 1017–1028, Sep. 1994.

[24] M. Hagedorn, P. Smith, P. Bones, R. Millane, and D. Pairman, "A trivariate chi-squared distribution derived from the complex Wishart distribution," *Journal of Multivariate Analysis*, vol. 97, no. 3, pp. 655–674, 2006.

Fusion of Evidences in Intensities Channels for Edge Detection in PolSAR Images

Anderson A. de Borba, Maurício Marengoni, and Alejandro C. Frery, *Senior Member, IEEE*

***Abstract*—Polarimetric Synthetic Aperture Radar (PolSAR) sensors have reached an essential position in remote sensing. The images they provide have speckle noise, making their processing and analysis challenging tasks. We discuss an edge detection method based on the fusion of evidences obtained in the intensity channels hh, hv, and vv of PolSAR multi-look images. The method consists of detecting transition points in the thinnest possible range of data that covers two regions using maximum likelihood under the Wishart distribution. The fusion methods used are: simple average, multi-resolution discrete wavelet transform (MR-DWT), principal component analysis (PCA), ROC statistics, multi-resolution stationary (MR-SWT) wavelet transform, and a multi-resolution method based on singular value decomposition (MR-SVD). A quantitative analysis suggests that PCA and MR-SVD provide the best results.**

***Index Terms*—PolSAR, edge detection, maximum likelihood estimation, fusion methods.**

I. Introduction

POLARIMETRIC synthetic aperture radar (PolSAR) has achieved an essential position in remote sensing. The data such sensors provide require specifically tailored signal processing techniques. Among such techniques, edge detection is one of the most important operations for extracting information. Edges are at a higher level of abstraction than mere data and, as such, provide relevant insights about the scene.

Among the available edge detection techniques for SAR and PolSAR images, it is worth mentioning: techniques based on denoising [1]–[4]; Markov random fields [5]; the deep learning approach [6] applied to segmentation and classification; and statistical techniques [7]–[9] applied in edge detection in PolSAR and SAR imagery.

This article follows the statistical modeling approach using the techniques described in [7]–[9] to find edge evidences, followed by fusion processes [10], [11].

Instead of handling fully polarimetric data, we treat each intensity channel separately, obtain evidence of edges, and then produce a single estimator of the edge position. With this, we quantify the contribution each channel provides to the solution of the problem.

The Gambini Algorithm [12] is an attractive edge detection technique. It is local, as it finds evidence of an edge over a thin strip of data; it works with any model, which makes it suitable for SAR data; and it has shown better performance than other approaches. This algorithm consists in casting rays, and then finding the evidence of an edge in the ray by maximizing a value function. We use the total likelihood of two samples: one inside the edge, another outside the edge. Without loss of generality, we assume the complex scaled Wishart distribution for the fully polarimetric observations, from which Gamma laws stem for each intensity channel. The value function depends on the estimates that index such Gamma laws; and we estimate them by maximum likelihood.

The total likelihood function is non-differentiable at most points, and classical methods have difficulties in finding its maximum. We used the Generalized Simulated Annealing (GenSA) [13] method to solve this problem.

We discuss and compare six fusion methods: Simple average [10], Multi-Resolution Discrete Wavelet, MR-DWT [14], Principal Component Analysis, PCA [10], [14], ROC statistics [15], Multi-Resolution Stationary Wavelet Transform, MR-SWT [14], [16], and Multi-Resolution Singular Value Decomposition, MR-SVD [17].

The article is structured as follows. Section II describes the models. Section III describes the edge detection. Section IV describes the approaches for fusing edge evidences. Section V presents the results. In Section VI we discuss the results, and outline future research directions.

II. Statistical modeling for PolSAR data

Multi-looked fully polarimetric data follow the Wishart distribution with PDF defined by:

$$f_{\mathbf{Z}}(\mathbf{z};\boldsymbol{\Sigma},L)=\frac{L^{pL}|\mathbf{z}|^{L-p}}{|\boldsymbol{\Sigma}|^{L}\Gamma_p(L)}\exp(-L\,\mathrm{tr}(\boldsymbol{\Sigma}^{-1}\mathbf{z})), \qquad (1)$$

where $\mathbf{z}$ is a positive-definite Hermitian matrix, L is the number of looks, $\mathrm{tr}(\cdot)$ is the trace operator of a matrix, $\Gamma_p(L)$ is the multivariate Gamma function defined by $\Gamma_p(L)=\pi^{\frac{1}{2}p(p-1)}\prod_{i=0}^{p-1}\Gamma(L-i)$, and $\Gamma(\cdot)$ is the Gamma function. We used three $p=3$ channels in this study. This situation is denoted by $\mathbf{Z}\sim W(\boldsymbol{\Sigma},L)$, which satisfies $E[\mathbf{Z}]=\boldsymbol{\Sigma}$. This assumption usually holds for fully developed speckle but, since we will estimate L locally instead of considering the same number of looks for the whole image, we will in part take into account departures from such hypothesis.

Since we are interested in describing the information conveyed by parts of such matrix under the Wishart model, we assume that the distribution of each intensity channel is a Gamma law with probability density function

$$f_Z(z;\mu,L)=\frac{L^L z^{L-1}}{\mu^L\Gamma(L)}\exp\big\{-Lz/\mu\big\},\quad z>0, \qquad (2)$$

A. A. de Borba is with the Dept. Engenharia Elétrica e Computação, Universidade Presbiteriana Mackenzie (UPM), and with IBMEC-SP, São Paulo, Brazil. anderson.borba@ibmec.edu.br

M. Marengoni is with the Dept. Engenharia Elétrica e Computação, UPM, São Paulo, Brazil. mauricio.marengoni@mackenzie.br

A. C. Frery is with the Laboratório de Computação Científica e Análise Numérica (LaCCAN), Universidade Federal de Alagoas (UFAL), Maceió, Brazil. acfrery@laccan.ufal.br

where $L > 0$, and $\mu > 0$ is the mean. The log-likelihood of the sample $\boldsymbol{z} = (z_1, \ldots, z_n)$ under this model is

$$\mathcal{L}(L, \mu; \boldsymbol{z}) = n\big[L \ln(L/\mu) - \ln \Gamma(L)\big] + L \sum_{k=1}^{n} \ln z_k - \frac{L}{\mu} \sum_{k=1}^{n} z_k. \tag{3}$$

We obtain $\big(\widehat{L}, \widehat{\mu}\big)$, the maximum likelihood estimator (MLE) of (L, μ) based on $\boldsymbol{z}$, by maximizing (3) with the BFGS method [18]. We prefer optimization to solving $\nabla \ell = \mathbf{0}$ for improved numerical stability.

III. Edge Detection on a Single Data Strip

The Gambini algorithm estimates the point at which the properties of a sample change. It has been used with stochastic distances [9], and with the likelihood function [7], [8] for edge detection in SAR/PolSAR imagery. It can be adapted to any suitable measure of dissimilarity between two samples.

The algorithm starts by casting rays from a point inside the candidate region, e.g., the centroid. Data are collected around each ray to form the sample $\boldsymbol{z} = (z_1, z_2, \ldots, z_n)$, which is partitioned at position j:

$$\boldsymbol{z} = (\underbrace{z_1, z_2, \ldots, z_j}_{\boldsymbol{z}_{\mathrm{I}}}, \underbrace{z_{j+1}, z_{j+2}, \ldots, z_n}_{\boldsymbol{z}_{\mathrm{E}}}).$$

We assume two (possibly) different models for each partition: $\boldsymbol{Z}_{\mathrm{I}} \sim \Gamma(\mu_{\mathrm{I}}, L_{\mathrm{I}})$, and $\boldsymbol{Z}_{\mathrm{E}} \sim \Gamma(\mu_{\mathrm{E}}, L_{\mathrm{E}})$. We then estimate $(\mu_{\mathrm{I}}, L_{\mathrm{I}})$ and $(\mu_{\mathrm{E}}, L_{\mathrm{E}})$ with $\boldsymbol{z}_{\mathrm{I}}$ and $\boldsymbol{z}_{\mathrm{E}}$, respectively, by maximizing (3), and obtain $\big(\widehat{\mu}_{\mathrm{I}}, \widehat{L}_{\mathrm{I}}\big)$ and $\big(\widehat{\mu}_{\mathrm{E}}, \widehat{L}_{\mathrm{E}}\big)$.

We then compute the total log-likelihood of $\boldsymbol{z}_{\mathrm{I}}$ and $\boldsymbol{z}_{\mathrm{E}}$:

$$\mathcal{L}\big(j; \widehat{\mu}_I, \widehat{L}_I, \widehat{\mu}_E, \widehat{L}_E\big) = -\left(\frac{\widehat{L}_{\mathrm{I}}}{\widehat{\mu}_{\mathrm{I}}} \sum_{k=1}^{j} z_k + \frac{\widehat{L}_{\mathrm{E}}}{\widehat{\mu}_{\mathrm{E}}} \sum_{k=j+1}^{n} z_k\right) +$$

$$j\big[\widehat{L}_{\mathrm{I}} \ln(\widehat{L}_{\mathrm{I}}/\widehat{\mu}_{\mathrm{I}}) - \ln \Gamma(\widehat{L}_{\mathrm{I}})\big] + \widehat{L}_{\mathrm{I}} \sum_{k=1}^{j} \ln z_k +$$

$$(n-j)\big[\widehat{L}_{\mathrm{E}} \ln(\widehat{L}_{\mathrm{E}}/\widehat{\mu}_{\mathrm{E}}) - \ln \Gamma(\widehat{L}_{\mathrm{E}})\big] + \widehat{L}_{\mathrm{E}} \sum_{k=j+1}^{n} \ln z_k. \tag{4}$$

and the estimate of the edge position on the ray is the coordinate $\widehat{j}$ which maximizes it.

Algorithm 1 is the pseudocode of the basic edge detection with the Gambini Algorithm. We found that one hundred rays is a good compromise between spatial continuity and computational load. Also, $\min_s$ is the minimum sample size.

In our implementation, we replace the exhaustive sequential search (the innermost **for** loop) by Generalized Simulated Annealing (GenSA [13]).

IV. Fusion of Evidences

Assume we have n_c binary images $\{\widehat{\boldsymbol{\jmath}}_c\}_{1 \le c \le n_c}$ in which 1 denotes an estimate of edge and 0 otherwise. They have common size $m \times n$; denote $\ell = mn$. These images will be fused to obtain the binary image $\boldsymbol{I}_F$.

We compare the results of six fusion techniques: simple average, multi-resolution discrete wavelet transform (MR-DWT), principal components analysis (PCA), ROC statistics, multi-resolution stationary wavelet transform (MR-SWT), and multi-resolution singular value decomposition (MR-SVD).

Data: n_c intensity channels, interior point, number of rays
Result: n_c binary images with evidences of edges
for *each band* $1 \le c \le n_c$ **do**
  for *each ray passing through the interior point* **do**
    $\boldsymbol{z} = (z_1, z_2, \ldots, z_n) \leftarrow$ data collected around the ray;
    for *each* $\min_s \le j \le n - \min_s$ **do**
      Partition the sample as $\boldsymbol{z}_{\mathrm{I}} = (z_{\min_s}, \ldots, z_j)$ and $\boldsymbol{z}_{\mathrm{E}} = (z_{j+1}, \ldots, z_{n-\min_s})$;
      Compute $\big(\widehat{\mu}_{\mathrm{I}}, \widehat{L}_{\mathrm{I}}\big)$ with $\boldsymbol{z}_{\mathrm{I}}$, and $\big(\widehat{\mu}_{\mathrm{E}}, \widehat{L}_{\mathrm{E}}\big)$ with $\boldsymbol{z}_{\mathrm{E}}$;
      Compute the total log-likelihood at j as $\mathcal{L}\big(j; \widehat{\mu}_I, \widehat{L}_I, \widehat{\mu}_E, \widehat{L}_E\big)$;
    end
    $\widehat{\jmath} \leftarrow$ the value of j which maximizes the total log-likelihood function;
    return $(\widehat{x}, \widehat{y})$, the coordinates of each $\widehat{\jmath}$;
  end
  return the binary image $\widehat{\boldsymbol{\jmath}}_c$ with 1 at every $(\widehat{x}, \widehat{y})$, and 0 otherwise.
end

Algorithm 1: Gambini algorithm for intensity channels

A. Simple Average

The simple average fusion method proposes the arithmetic mean of the edge evidence in each of the n_c channels: $\boldsymbol{I}_F(x, y) = (n_c)^{-1} \sum_{c=1}^{n_c} \widehat{\boldsymbol{\jmath}}_c(x, y)$, where $1 \le x \le m$ indexes the rows, and $1 \le y \le n$ the columns of the image.

B. Multi-Resolution Discrete Wavelet – MR-DWT

This section is based on [14]. We apply DWT filters on each binary image $\widehat{\boldsymbol{\jmath}}_c$: a low-pass filter $\boldsymbol{L}$ in the vertical direction, and a high-pass filter $\boldsymbol{H}$ in the horizontal direction, then both are down-sampled to create the coefficient matrices $\widehat{\boldsymbol{\jmath}}_{c\mathrm{L}}$ and $\widehat{\boldsymbol{\jmath}}_{c\mathrm{H}}$. These operations are repeated on the coefficient matrices, leading to $\widehat{\boldsymbol{\jmath}}_{c\mathrm{LL}}$, $\widehat{\boldsymbol{\jmath}}_{c\mathrm{LH}}$, $\widehat{\boldsymbol{\jmath}}_{c\mathrm{HL}}$, and $\widehat{\boldsymbol{\jmath}}_{c\mathrm{HH}}$. We, thus, use two resolution levels.

The DWT fusion method has the following steps:

1) Calculate the DWT decomposition $\widehat{\boldsymbol{\jmath}}_{c\mathrm{LL}}$, $\widehat{\boldsymbol{\jmath}}_{c\mathrm{LH}}$, $\widehat{\boldsymbol{\jmath}}_{c\mathrm{HL}}$, and $\widehat{\boldsymbol{\jmath}}_{c\mathrm{HH}}$, for each channel.
2) Compute $\overline{\boldsymbol{\jmath}}_{c\mathrm{HH}}$, the pixel-wise mean of all $\widehat{\boldsymbol{\jmath}}_{c\mathrm{HH}}$ decompositions.
3) Find the pixel-wise maximum of $\widehat{\boldsymbol{\jmath}}_{c\mathrm{LL}}$, $\widehat{\boldsymbol{\jmath}}_{c\mathrm{LH}}$, $\widehat{\boldsymbol{\jmath}}_{c\mathrm{HL}}$: $\overline{\boldsymbol{\jmath}}_{c\mathrm{LL}}$, $\overline{\boldsymbol{\jmath}}_{c\mathrm{LH}}$, and $\overline{\boldsymbol{\jmath}}_{c\mathrm{HL}}$.
4) The result of the fusion I_F is the inverse DWT transform of the coefficient matrices $\overline{\boldsymbol{\jmath}}_{c\mathrm{HH}}$, $\overline{\boldsymbol{\jmath}}_{c\mathrm{LL}}$, $\overline{\boldsymbol{\jmath}}_{c\mathrm{LH}}$, and $\overline{\boldsymbol{\jmath}}_{c\mathrm{HL}}$.

C. Principal Component Analysis – PCA

This section is based on [10], [14]. The method is comprised of the following steps:

1) Stack the binary images $\widehat{\boldsymbol{\jmath}}_c$ in column vectors to obtain the matrix $\boldsymbol{X}_{\ell \times n_c}$.
2) Calculate the covariance matrix $\boldsymbol{C}_{n_c \times n_c}$ of $\boldsymbol{X}_{\ell \times n_c}$.

3) Compute the matrices of eigenvalues ($\boldsymbol{\Lambda}$) and eigenvectors ($\boldsymbol{V}$) of the covariance matrix, sorted in decreasing order by the eigenvalues.
4) Compute the vector $\boldsymbol{P} = (P(1), \ldots, P(n_c)) = (\sum_{c=1}^{n_c} V(c))^{-1}\boldsymbol{V}$, where $\boldsymbol{V}$ is eigenvector associated with the highest eigenvalue of $\boldsymbol{C}_{n_c \times n_c}$; notice that $\sum_{c=1}^{n_c} P(c) = 1$.
5) Fuse $\boldsymbol{I}_F(x,y) = \sum_{c=1}^{n_c} P(c)\widehat{\boldsymbol{\jmath}}_c(x,y)$.

D. ROC Statistics

The ROC method was proposed and described on [15]:

1) Add the binary images $\widehat{\boldsymbol{\jmath}}_c$ to produce the frequency matrix ($\boldsymbol{V}$).
2) Use thresholds ranging from $t = 1, \ldots, n_c$ on $\boldsymbol{V}$ to generate matrices $\boldsymbol{M}_t$.
3) Compare each $\boldsymbol{M}_t$ with all $\widehat{\boldsymbol{\jmath}}_c$, find the confusion matrix to generate the ROC curve. The optimal threshold corresponds to the point of the ROC curve closest (in the sense of the Euclidean distance) to the diagnostic line.
4) The fusion $\boldsymbol{I}_F$ is the matrix $\boldsymbol{M}_t$ which corresponds to the optimal threshold.

E. Multi-Resolution Stationary Wavelet Transform – MR-SWT

This section is based on [14], [16]. The difference between MR-DWT and MR-SWT method is the replacement of the Discrete Wavelet Transform (DWT) by the Stationary Wavelet Transform SWT.

F. Multi-Resolution Singular Value Decomposition – MR-SVD

MR-SVD Fusion [17] works similarly to MR-DWT. The MR-SVD fusion method can be summarized as follows:

1) Organize the binary image $\widehat{\boldsymbol{\jmath}}_c$ as non-overlapping 2×2 blocks, and arrange each block as a 4×1 vector by stacking columns to form the data matrix $\boldsymbol{X}_1$ with dimension $4 \times \ell/4$.
2) Find the SVD decomposition of $\boldsymbol{X}_1 = \boldsymbol{U}_1\boldsymbol{S}_1\boldsymbol{V}_1^T$, where $\boldsymbol{U}_1$ is a 4×4 unitary matrix, $\boldsymbol{S}_1$ is a $4 \times \ell/4$ rectangular diagonal matrix known as singular values matrix, and $\boldsymbol{V}_1$ is an $\ell/4 \times \ell/4$ unitary matrix. The singular values are ordered in a decreasing order.
3) Transform the lines of $\widehat{\boldsymbol{X}_1} = \boldsymbol{U}_1^T\boldsymbol{X}_1 = \boldsymbol{S}_1\boldsymbol{V}_1^T$ into new matrices with dimensions $m/2 \times n/2$: $\{\boldsymbol{\Phi}_1, \boldsymbol{\Psi}_{1\mathrm{V}}, \boldsymbol{\Psi}_{1\mathrm{H}}, \boldsymbol{\Psi}_{1\mathrm{D}}\}$.
4) Repeat the procedure (1) on $\boldsymbol{\Phi}_r$ by $r = 2$ up to the lowest resolution level R.
5) The MR-SVD decomposition in each channel is

$$\widehat{\boldsymbol{X}_c} \rightarrow \left\{\boldsymbol{\Phi}_{\mathrm{R}}^c, \{\boldsymbol{\Psi}_{r\mathrm{V}}^c, \boldsymbol{\Psi}_{r\mathrm{H}}^c, \boldsymbol{\Psi}_{r\mathrm{D}}^c\}_{r=1}^{\mathrm{R}}, \{\boldsymbol{U}_r^c\}_{r=1}^{\mathrm{R}}\right\}.$$

6) Once the decomposition is applied to all channels, compute the average of $\boldsymbol{\Phi}_R^c$ ($\boldsymbol{\Phi}_{\mathrm{R}}^f$) in the lowest resolution level, and the average of $\boldsymbol{U}_r^c$ ($\boldsymbol{U}_{\mathrm{r}}^f$), for each r, where f denotes the fusion among channels.
7) Find the pixel-wise maxima of $\boldsymbol{\Psi}_{r\mathrm{V}}^c$, $\boldsymbol{\Psi}_{r\mathrm{H}}^c$ and $\boldsymbol{\Psi}_{r\mathrm{D}}^c$: $\boldsymbol{\Psi}_{rV}^f$ $\boldsymbol{\Psi}_{r\mathrm{V}}^f$, $\boldsymbol{\Psi}_{r\mathrm{H}}^f$ and $\boldsymbol{\Psi}_{r\mathrm{D}}^f$.
8) The fusion $\boldsymbol{I}_F$ is the SVD transformation for each level $r = \mathrm{R}, \ldots, 1$,

$$\boldsymbol{I}_F \leftarrow \left\{\boldsymbol{\Phi}_{\mathrm{R}}^f, \{\boldsymbol{\Psi}_{r\mathrm{V}}^f, \boldsymbol{\Psi}_{r\mathrm{H}}^f, \boldsymbol{\Psi}_{r\mathrm{D}}^f\}_{r=\mathrm{R}}^{1}, \{\boldsymbol{U}_r^f\}_{r=\mathrm{R}}^{1}\right\}.$$

We also used two resolution levels.

V. Results

A. Flevoland images

Fig. 1(a) shows a 750×1024 pixels AIRSAR PolSAR image of Flevoland, L-band, with the radial lines where edges are detected. Fig. 1(b) shows the ground reference in red.

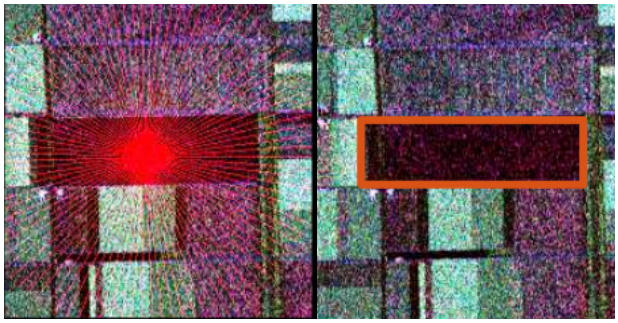

(a) Image and rays. (b) Ground reference

Fig. 1. Flevoland image in Pauli decomposition, and ground reference

Figs. 2(a), 2(b), and 2(c) show, respectively, the edge evidences in the hh, hv and vv channels as obtained by MLE.

It is worth noting that GenSA has accurately identified the maximum value of $\mathcal{L}$ (Eq. (4)), even in the presence of multiple local maxima. A visual assessment leads to conclude that the best results are provided by hv, although with a few points far from the actual edge.

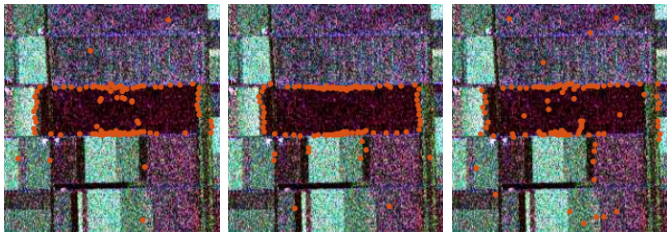

(a) Channel hh (b) Channel hv (c) Channel vv

Fig. 2. Edges evidences from the three intensity channels

Figs. 3(a), 3(b), 3(c), 3(d), 3(e), and 3(f) show the results of fusing these evidences.

Simple average and PCA produce similar results. MR-SVD produces considerably less outliers than the other methods. ROC produces accurate edges, with few outliers, but sparsely. Both wavelet-based methods (DWT and SWT) produce too dense edges and many outliers.

Fig. 4 shows another region in the Flevoland image. In this case, it is a bright target surrounded by darker fields. Fig. 5 shows the edges detected in each intensity channel and, again, the hv data are the one which produce the most accurate results.

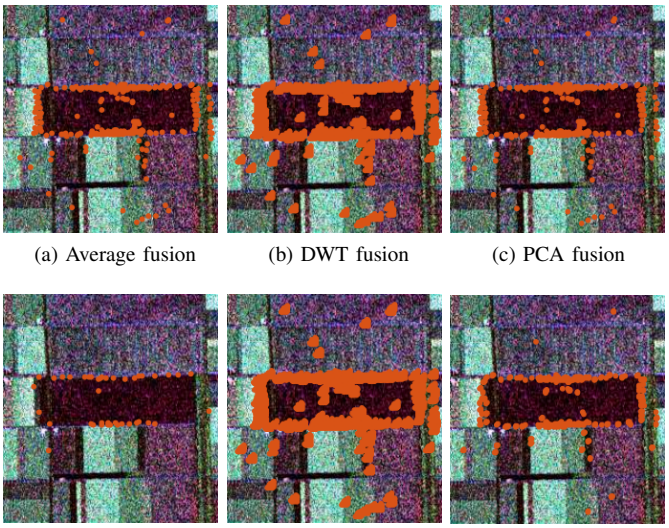

(a) Average fusion (b) DWT fusion (c) PCA fusion

(d) ROC fusion (e) MR-SWT fusion (f) MR-SVD fusion

Fig. 3. Results of applying the six fusion methods

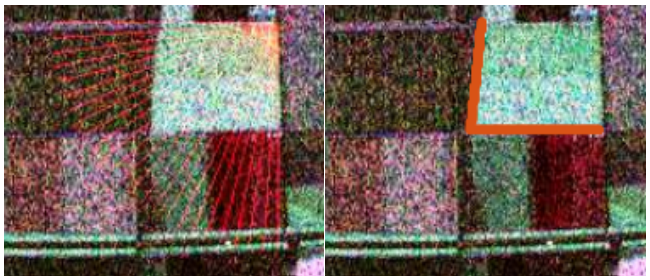

(a) Image and rays. (b) Ground reference

Fig. 4. Flevoland image in Pauli decomposition, and ground reference

Fig. 6 shows the two best fusion results: PCA and MR-SVD. Notice that the latter (Fig. 6(b)) eliminates the wrong detection close to the center of the area, and has fewer wrongly detected points outside the region of interest.

B. San Francisco Image

Fig. 7 shows an area of an L-band AIRSAR image over San Francisco. The distinctive areas are urban, sea, and vegetation. The aim is finding the edge between the former and the other two.

Fig. 8 shows the evidences of edges found in each of the three intensity channels. A visual inspection suggests that the hh channel is the one that produces the best estimation.

(a) Channel hh (b) Channel hv (c) Channel vv

Fig. 5. Edges evidences from the three intensity channels, Flevoland image

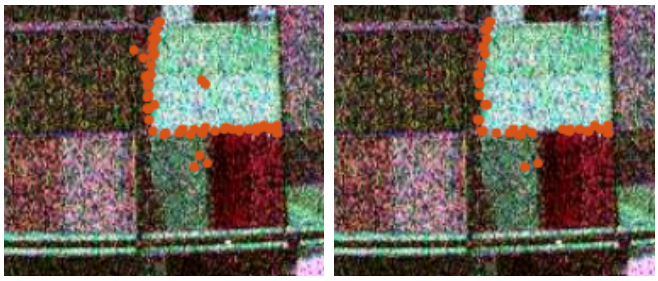

(a) PCA fusion (b) MR-SVD fusion

Fig. 6. Two best fusion results in the Flevoland image

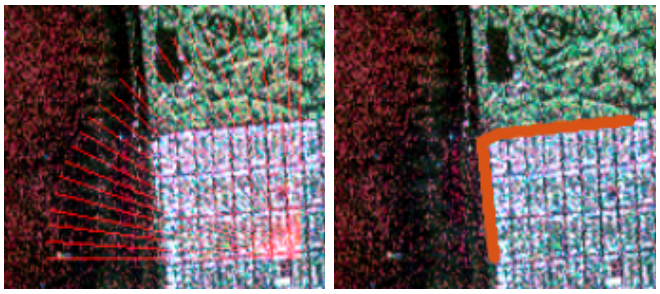

(a) Image and rays. (b) Ground reference

Fig. 7. San Francisco image in Pauli decomposition, and ground reference

Fig. 9 shows the two best fusion results: PCA and MR-SVD. Again, the latter is more resistant to outliers, both inside and outside the region of interest.

C. Error analysis

Figure 10 shows the error of $\widehat{j}$ in finding the true edge shown in Fig. 1(b), as measured on 100 lines with the minimum Euclidean distance between the ground truth and the detected

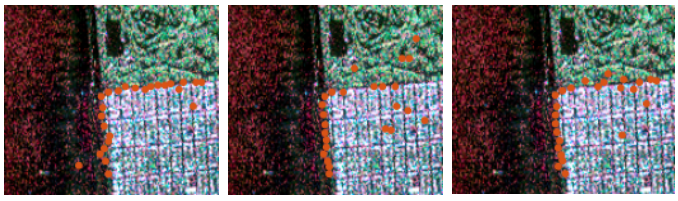

(a) Channel hh (b) Channel hv (c) Channel vv

Fig. 8. Edges evidences from the three intensity channels to San Francisco

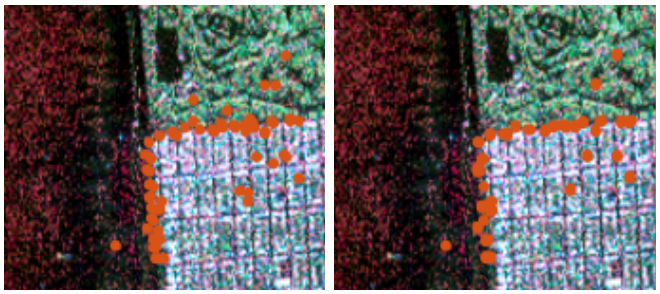

(a) PCA fusion (b) MR-SVD fusion

Fig. 9. Two best fusion results in the San Francisco image

pixel in the fusion methods. We use relative frequencies to estimate the probability of having an error smaller than a number of pixels. Denoting $H(k)$ the number of lines for which the error is less than k pixels, an estimate of this probability is $f(k) = H(k)/n_r$, where n_r is number of lines. In our analysis, k varies between 1 and 10, and $n_r = 100$. The algorithm is described in Ref. [8].

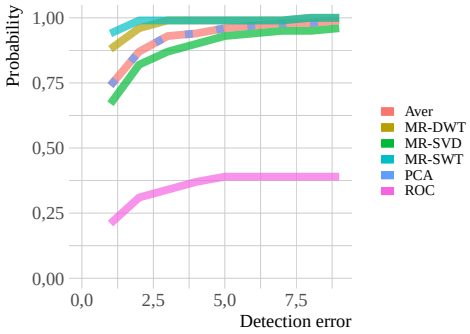

Fig. 10. Probability of detecting the edge by the fusion methods in Fig. 1.

We obtained similar results on the images shown in Figs. 4 and 7, which we omit for brevity.

D. Implementation Details

Table I shows the running times (absolute and relative to the fastest method). The system presented here was executed on a Intel© Core i7-9750HQ CPU 2.6 GHz 16 GB RAM computer.

TABLE I
PROCESSING TIMES (FUSION METHOD).

Method	Aver.	PCA	MR-DWT	MR-SWT	ROC	MR-SVD
Time (s)	0.01	0.02	0.08	0.18	0.40	1.11
Rel. time	1.00	2.19	9.25	21.05	46.59	129.57

The method for detecting edge evidence MLE was implemented in the R language. The fusion methods were implemented in Matlab. Code and data are available at https://github.com/anderborba/Code_GRSL_2020_1.

VI. Conclusion

We found evidence of edges using the maximum likelihood method under the Wishart model for PolSAR data. The evidence was found in each of the three intensity channels of AIRSAR L-band images over Flevoland and San Francisco.

Over the agricultural fields of Flevoland, the best edge evidence was observed on the hv channel. The hh channel provided the best estimates of the edges between the urban and both sea and vegetation areas of San Francisco. Such diversity of information content justifies the need of fusing the edge evidences.

We applied simple average, MR-DWT, PCA, ROC, MR-SWT, and MR-SVD fusion methods to aggregate the evidence obtained in the three channels. The best results were produced by PCA and by the Multi-Resolution Singular Value Decomposition (MR-SVD). Such enhancement comes at additional computational cost in terms of processing time.

We quantitatively assessed the results by checking the closeness of the fused points to the actual edge, and by the presence of outliers. Although the average and PCA are similar with respect to the probability of correctly detecting the edge, the latter provides a more effective weight of the evidences. In fact, PCA is able to completely discard misleading evidences, while the average cannot.

Two avenues for future improvement of the fusion are: (1) increasing the number of evidences. This is possible, since fully polarimetric data are richer than mere intensity channels; and (2) post-processing of both partial evidences and fusion.

References

[1] J. Shi, H. Jin, and Z. Xiao, "A novel hybrid edge detection method for polarimetric SAR images," *IEEE Access*, vol. 8, pp. 8974–8991, 2020.
[2] B. Liu, Z. Zhang, X. Liu, and W. Yu, "Edge extraction for polarimetric SAR images using degenerate filter with weighted maximum likelihood estimation," *IEEE Geosci. Remote Sens. Lett.*, vol. 11, no. 12, pp. 2140–2144, Dec 2014.
[3] W. Wang, D. Xiang, Y. Ban, J. Zhang, and J. Wan, "Enhanced edge detection for polarimetric SAR images using a directional span-driven adaptive window," *Int. J. Remote Sens.*, vol. 39, no. 19, pp. 6340–6357, 2018.
[4] D. Santana-Cedrés, L. Gomez, L. Alvarez, and A. C. Frery, "Despeckling PolSAR images with a structure tensor filter," *IEEE Geosci. Remote Sens. Lett.*, vol. 17, no. 2, pp. 357–361, Feb 2020.
[5] F. Baselice and G. Ferraioli, "Statistical edge detection in urban areas exploiting SAR complex data," *IEEE Geosci. Remote Sens. Lett.*, vol. 9, no. 2, pp. 185–189, March 2012.
[6] X. X. Zhu, D. Tuia, L. Mou, G. Xia, L. Zhang, F. Xu, and F. Fraundorfer, "Deep learning in remote sensing: A comprehensive review and list of resources," *IEEE Geosci. Remote Sens. Mag.*, vol. 5, no. 4, pp. 8–36, Dec 2017.
[7] J. Gambini, M. Mejail, J. Jacobo-Berlles, and A. C. Frery, "Feature extraction in speckled imagery using dynamic B-spline deformable contours under the G0 model," *Int. J. Remote Sens.*, vol. 27, no. 22, pp. 5037–5059, 2006.
[8] A. C. Frery, J. Jacobo-Berlles, J. Gambini, and M. Mejail, "Polarimetric SAR image segmentation with B-Splines and a new statistical model," *Multidimension. Syst. Signal Process.*, vol. 21, pp. 319–342, 2010.
[9] A. Nascimento, M. Horta, A. Frery, and R. Cintra, "Comparing edge detection methods based on stochastic entropies and distances for PolSAR imagery," *IEEE J. Sel. Topics Appl. Earth Observ. Remote Sens.*, vol. 7, no. 2, pp. 648–663, 2014.
[10] H. Mitchell, *Image Fusion: Theories, Techniques and Applications*. Springer Berlin Heidelberg, 2010.
[11] A. A. de Borba, M. Marengoni, and A. C. Frery, "Fusion of evidences for edge detection in PolSAR images," in *2019 IEEE Recent Advances in Geoscience and Remote Sensing: Technologies, Standards and Applications (TENGARSS)*, Oct 2019, pp. 80–85.
[12] J. Gambini, M. Mejail, J. Jacobo-Berlles, and A. C. Frery, "Accuracy of edge detection methods with local information in speckled imagery," *Statistics and Computing*, vol. 18, no. 1, pp. 15–26, 2008.
[13] Y. Xiang, S. Gubian, B. Suomela, and J. Hoeng, "Generalized Simulated Annealing for Global Optimization: The GenSA Package," *The R Journal*, vol. 5, no. 1, pp. 13–28, 2013.
[14] V. Naidu and J. Raol, "Pixel-level image fusion using wavelets and principal component analysis," *Defence Science Journal*, vol. 58, pp. 338–352, Mar. 2008.
[15] S. Giannarou and T. Stathaki, "Optimal edge detection using multiple operators for image understanding," *EURASIP Journal on Advances in Signal Processing*, vol. 2011, no. 1, p. 28, Jul 2011.
[16] Q. Jiang, X. Jin, S. Lee, and S. Yao, "A novel multi-focus image fusion method based on stationary wavelet transform and local features of fuzzy sets," *IEEE Access*, vol. 5, pp. 20 286–20 302, 2017.
[17] V. Naidu, "Image fusion technique using multi-resolution singular value decomposition," *Defence Science Journal*, vol. 61, no. 5, pp. 479–484, Sep. 2011.
[18] A. Henningsen and O. Toomet, "maxlik: A package for maximum likelihood estimation in R," *Computational Statistics*, vol. 26, no. 3, pp. 443–458, 2011.